A switchable pH-differential unitized regenerative fuel cell with high performance

A switchable pH-differential unitized regenerative fuel cell with high performance

Xu Lu,[a] Jin Xuan,[be] Dennis Y.C. Leung,[*a] Haiyang Zou,[a] Jiantao Li,[ac] Hailiang Wang [d] and Huizhi Wang [*b]

[a] Department of Mechanical Engineering, The University of Hong Kong, Pok Fu Lam, Hong Kong

[b] Institute of Mechanical, Process and Energy Engineering, School of Engineering and Physical Sciences, Heriot-Watt University, Edinburgh, EH14 4AS, UK

[c] SINOPEC Fushun Research Institute of Petroleum and Petrochemicals, Fushun, China

[d] Department of Chemistry, Yale University, West Haven, CT, United States

[e] State-Key Laboratory of Chemical Engineering, School of Mechanical and Power Engineering, East China University of Science and Technology, Shanghai 200237, China

Correspondence and requests for materials should be addressed to D.Y.C.L. (email: ycleung@hku.hk) or to H.Z.W. (email: h.wang@hw.ac.uk).

Abstract

Regenerative fuel cells are a potential candidate for future energy storage, but their applications are limited by the high cost and poor round-trip efficiency. Here we present a switchable pH-differential unitized regenerative fuel cell capable of addressing both the obstacles. Relying on a membraneless laminar flow-based design, pH environments in the cell are optimized independently for different electrode reactions and are switchable together with the cell process to ensure always favorable thermodynamics for each electrode reaction. Benefiting from the thermodynamic advantages of the switchable pH-differential arrangement, the cell allows water electrolysis at a voltage of 0.57 V, and a fuel cell open circuit voltage of 1.89 V, rendering round-trip efficiencies up to 74%. Under room conditions, operating the cell in fuel cell mode yields a power density of 1.3 W cm^{-2}, which is the highest performance to date for laminar flow-based cells and is comparable to state-of-the-art polymer electrolyte membrane fuel cells.

Keywords

pH-differential technique

Hydrogen/oxygen regenerative fuel cell

Microfluidic reactor

High performance

Heat management

Cyclic operation

1 Introduction

The pursuit of a low-carbon future with increasing mobility urges the development of high-capacity, efficient and affordable energy storage technologies for a range of applications including portable electronics, electrical vehicles and stationary grid storage. Hydrogen and fuel cells have long been considered as a solution in this regard, because hydrogen has the highest specific energy and fuel cells provide the most versatile, efficient and cleanest way for the conversion of hydrogen energy. When used for energy storage, fuel cells are combined with a water electrolyzer, to form a so-called regenerative fuel cell (RFC), which converts electrical energy to hydrogen and oxygen, and then converts the fuels by fuel cell reactions back to electricity as needed. However, the practical implementation of RFCs has been hampered by their poor round-trip efficiency (50~60% vs. 60~95% for secondary batteries)[1] and the high cost of fuel cells ($10,000 kW^{-1} vs. $300~4000 kW^{-1} for batteries)[2], which can be primarily ascribed to the sluggish kinetics at the oxygen electrode. The high overpotential originated from the intrinsically slow kinetics of oxygen evolution / reduction reactions seriously impairs the round-trip efficiencies and necessitates the use of expensive noble metal catalysts that are a proven major contributor to the cell cost[3]. To address the obstacles, we and other researchers have devoted much effort either to enhancing the platinum mass activity[4, 5] or to exploiting non-noble alternatives[6-9]. Nevertheless, neither of the ways circumvents cost and performance compromise. Alternatively, replacing the oxygen electrode with more facile reactions leads to a significant reduction of overpotentials. Performance breakthroughs have been recently demonstrated in a hydrogen / bromine cell using aqueous bromine instead of oxygen as an oxidant[10], as well as a water electrolyzer relying on ethanol oxidation instead of oxygen evolution at the anode[11]. Yet, no substitute species is expected to be as good as oxygen in terms of availability and safety.

Here we propose to address the aforementioned issues by developing a switchable pH-differential unitized regenerative fuel cell (s-URFC). The novelty of this work lies in the following aspects: (i) pH environments are optimized from the thermodynamic point of view independently for different anode and cathode reactions, and they are switchable when the cell process is reversed to ensure always favourable pH conditions for each electrode reaction. By doing this, the cell performance and round-trip efficiency are substantially enhanced; (ii) a unitized configuration that combines the functionality of a fuel cell and an electrolyzer in a single device is applied in the present cell, allowing for a significant reduction in the system weight and cost. This unitized-type operation is enabled with a membraneless laminar flow-based platform[12, 13], which itself also helps reduce the cost by eliminating the need of a membrane electrode assembly. In fuel cell (FC) mode, the hydrogen side (i.e. anode) is paired with high pH (i.e. alkaline) and the oxygen side (i.e. cathode) is paired with low pH (i.e. acid), hence raising the thermodynamically determined output voltages. In electrolysis (EL) mode, pHs the electrolytes are switched. The oxygen evolution reaction occurs at the anode side with alkaline anolyte and the hydrogen evolution reaction occurs at the cathode side with acid catholyte, resulting in a thermodynamically lowered applied voltage. Enjoying the thermodynamic benefits of different pH differential arrangements in its different operating modes (i.e. the FC and EL mode), the s-URFC allows water spitting at a voltage of 0.57 V (half those of conventional electrolyzers), and a fuel cell open circuit voltage (OCV) of 1.89 V (nearly twice those of conventional hydrogen/oxygen fuel cells), rendering round-trip efficiencies up to 74%. Under room conditions, the operation of the cell in the FC mode delivers a current density of 3.6 A cm^{-2} and power density of 1.3 W cm^{-2}, which is the highest performance to date for laminar flow-based electrochemical cells and is comparable to state-of-the-art practices of polymer electrolyte membrane (PEM) fuel cells.

2 Experimental

2.1 Cell fabrication and assembly

The anode and cathode of the cell were made of PTFE-hydrophobized carbon paper (HCP120, Hesen) with PtRu/C (60 wt.% Pt, 30 wt% Ru, Johnson Matthey) loading of 4 mg cm^{-2}. The two electrodes were housed between two 0.5-mm-thick polyvinyl chloride (PVC) plates with a 0.2 (W) × 0.5 (L) cm^2 window cut out to define the reactive area. Two 0.1-mm-thick PVC plates were used to separate the electrodes and create identical anolyte and catholyte channels of 0.2 (W) × 7.5 (L) cm^2, between which another 0.1-mm-thick PVC plate with a 0.2 (W) × 0.5 (L) cm^2 window was sandwiched to form the electrolyte contact area. Two 5 (L) × 1 (W) × 0.5 (H) cm^3 PVC chambers were fabricated to be gas channels. All layered components were fabricated using a carbon dioxide laser ablation system (VLS 2.30, Universal Laser System) and clamped together by binder clips (Highmark). Prior to the experiments, a leakage test was carried out by immersing the cell into a beaker filled with water when passing nitrogen through the gas channels.

2.2 Electrochemistry

All the electrochemical tests were performed under ambient conditions using a CHI 660E electrochemical station. Charge and discharge profiles were respectively obtained by chronopotentiometry and chronoamperometry techniques under galvanostatic and potentiostatic control. Each data point is an average value over a run time of 25 s. In the meantime, potentials of each individual electrode were recorded with digital multi-meters (Fluke) connected between each electrode and an external Ag/AgCl reference electrode in the exit electrolyte stream. The current and power outputs were normalized to the geometric surface area of electrodes (i.e. 0.1 cm^2). For the cell operation, 3 M H_2SO_4 and 3 M KOH were respectively employed as the acid and alkaline electrolytes, and they were supplied to the cell

using a dual syringe pump (LSP02-1B, Longer Pump) at a stream flow rate of 1400 μL min^{-1}. Hydrogen (≥ 99.995%, Linde) and oxygen (≥ 99.5%, Linde) in FC mode were respectively fed into the anode and cathode gas channels at a flow rate of 100 mL min^{-1} controlled by a mass flow controller (GFC17, Aalborg). Cyclic voltammetry (CV) measurements of the PtRu/C catalysts were conducted under N_2-saturated conditions at a scan rate of 100 mV s^{-1} in the voltage window of 0 ~ 0.6 V for 3 M H_2SO_4 and -0.9 ~ 0.1 V for 3 M KOH in a three-electrode configuration, where a Hg/Hg_2SO_4 (Sat. K_2SO_4) (for acid) or Hg/HgO (3 M KOH) (for alkali) was used as the reference electrode, and a platinum foil was used as the counter electrode. Morphological characterization of the electrocatalysts before or after cycling was performed with a Hitachi S-4800 SEM and FEI Tecnai G2 TEM. All experiments reported here were conducted at atmospheric pressure (1 atm) and room temperature (ca. 24℃).

2.3 Fluorescent dye characterization

We dissolved 0.25 mM fluorescein sodium salt ($C_{20}H_{10}Na_2O_5$, Sigma-Aldrich) in the streams of anolyte and catholyte as a pH-sensitive fluorescent dye. The fluorescent dye was excited using a blue light source at a wavelength of 460-490 nm (Intensilight C-HGFI, Nikon). At this wavelength, the absorbance of $C_{20}H_{10}Na_2O_5$ is nearly independent of the pH value, whereas the emission increases with increasing pH. For calibration, the emitted light intensity was recorded as buffer solutions ranging from pH -0.09 to pH 14.11 flowed through the microchannel (Figure S1). The fluorescence images were acquired using an inverted fluorescence microscope with 4× objective (Eclipse TE2000-U, Nikon). The gain remained constant at 1 and the exposure time was fixed at 60 ms.

2.4 Temperature measurements

The temperature distribution within the microchannel was acquired using a thermal infrared microscope (FSV-GX7700, Apiste) together with 4-fold magnification near-infrared objective lens. Prior to the measurements, the measurement setup was calibrated with a water thermostat (RCT basic, IKA Labortechnik) as water at given temperatures of 43, 40, 38, 36, 34, 32 and 30 ^{o}C was circulated in the cell. A maximum error of 0.7 ^{o}C was detected due to inevitable heat loss. Note that all microscopy analyses in this study were performed with a cell specially designed to facilitate the optical observation (Figure S2).

3 Results

3.1 Design and working principles

Figure 1(a) shows the Pourbaix diagram of water where the Nernst potentials of oxygen and hydrogen electrodes are plotted against pH values. Knowing that for a reaction $aA + bB \leftrightharpoons gG + hH$ with a corresponding Nernst equation $E = E^0 - \frac{RT}{zF}\ln\frac{{c_G}^g {c_H}^h}{{c_A}^a {c_B}^b}$, for the case of H_2/O_2 regenerative fuel cell, the hydrogen evolution reaction corresponds to the Nernst equation $E_{H^+/H_2} = E^0_{H^+/H_2} + \frac{RT}{nF}\ln(\frac{[H^+]^2}{P_{H_2}})$ and the oxidation of water corresponds to $E_{O_2/H_2O} = E^0_{O_2/H_2O} + \frac{RT}{nF}\ln(P_{O_2}[H^+]^4)$. Alternating temperature and pressure in a membraneless cell would require extra energy input and invovle high-cost cell materials for fabrication. In addition, a temperature difference of $100℃$ can only achieve a voltage adjustment of 0.02V, indicating the low feasibility on microfluidic or polymer exchange membrane fuel cells operating below $200℃$. Therefore, under ambient condition, i.e. keeping the temperature and pressure constant, the individual potentials of the oxygen and hydrogen electrodes drop linearly with the logarithm of H^+ concentration, i.e. the pH, whereas the thermodynamic stability window of water remains unaltered at 1.229 V (the green region in Figure 1(a)) when the two electrodes are shifted by the same amount in pH as in the conventional single electrolyte

systems. The basic idea behind the work is to alter the thermodynamic limit of 1.229 V respectively for the different operating modes of a RFC by pairing its two electrodes in two electrolytes of different pH values, thus maximizing performance and round-trip efficiency. Higher voltages are attained in the FC mode by applying an acid oxygen electrode and alkaline hydrogen electrode, whereas lower charging voltages in the EL mode are achieved by reversing the pH environments for the two electrodes. Figure 1(b) presents a schematic diagram of the new system in which two pumps are incorporated for the circulation of the acid and alkaline electrolytes together with a rotary valve for easy switching between them. The key challenge, however, lies in how to combine different pH-differential strategies in a single set of hardware, as the anion / proton exchange bipolar membrane (BPM) used in conventional hybrid systems to separate the acid and alkaline electrolytes is specific to the type of ions passing through it, such that a pH switch between the two sides of the membrane is not possible unless the BPM configuration is changed[14, 15]. To overcome the challenge, the present cell unit employed a laminar flow-based fuel cell platform detailed elsewhere[12], where the alkaline anolyte and acid catholyte streams flow in parallel along a single microchannel with an anode and a cathode on opposing side walls. The laminar nature of microchannel flow limits the mixing of the two electrolytes only to diffusion at the stream interface, thereby preventing bulk acid-base neutralization without the need for a BPM. The membraneless design was well validated under a fluorescent microscope using a pH sensitive fluorescent probe, which indicates a clear interface and a good separation of the electrolytes for both FC and EL operation (Figure 1(c)). In the paper, the cell performances were studied using 3 M H_2SO_4 (pH ~ -0.48) and 3 M KOH (pH ~ 14.48) respectively as the catholyte and anolyte. The cell electrodes were gas diffusion electrodes (GDEs) with PtRu/C reversible bifunctional catalysts which have shown reasonable activity towards reactions of oxygen evolution / reduction and hydrogen evolution / oxidation[16, 17]. The hydrogen and oxygen gases necessary for the FC operation were forced

convectively through two PVC gas chambers on the outside of the GDEs. Table 1 summarizes the reactions that occur in the s-URFC, and their associated reactant flows are shown in Figure 1(c). Theoretically, our s-URFC has a charging voltage of 0.347 V and a discharge voltage of 2.111 V, corresponding to a voltage efficiency (i.e., the ratio of discharge to charge voltages) [10] over 6. Compared to single-pH regenerative systems, the larger-than-one voltage efficiency in the proposed new cell is a result of electrochemical neutralization, where the acid and base are consumed separately at the cathode and anode, directly converting the free energy of water formation ($H^+ + OH^- \leftrightarrow H_2O$) into voltage ($\Delta G = -FU_{\Delta pH} = -RT \ln (a_{H+}a_{OH-})^{-1}$, with $U_{\Delta pH}$ = 0.882 V for 3 M acid and 3 M base at 25 ºC). The liquid junction potential formed at the acid-base interface is estimated from the Henderson equation[18] to be 37 mV at maximum, and thus has negligible effects on the cell performance.

3.2 High-power operation

The discharge data of the s-URFC is plotted and compared to its single-pH counterparts under analogous conditions in Figure 2(a). The s-URFC exhibits an OCV at 1.89 V, which is 63 to 87% higher than that of the single-pH cells (1.16 V for the alkaline cell, and 1.01 V for the acid cell). The deviation in the OCVs in both the cases of s-URFC and single-pH cells from their calculated thermodynamic values is likely due to the mixed potential formation on the Pt/PtO catalytic surface[19]**.** The maximum current and power densities of the s-URFC are respectively 3.6 A cm^{-2} and 1.3 W cm^{-2}, in contrast, the single-pH cells are operated below 0.52 W cm^{-2}. Not surprisingly, the single-acid cell yields 55% higher power density than the single-alkaline cell primarily due to much superior anode performance in acid media[20]. To further understand the remarkable performance improvement with the new cell, the in-situ polarization behavior of each individual electrode is shown in Figure 2(b). The s-URFC is seen to have both its electrodes operated with an optimal thermodynamics, but its electrode kinetics are not

optimal. The overpotentials of both the oxygen reduction and hydrogen oxidation in alkaline is larger than those in acid electrolyte. Figure 2(c) compares the present cell performance with other existing membraneless laminar flow-based electrochemical cells[10, 18, 21-33]. The present power density nearly doubles the highest previously reported power density for laminar flow-based cells, which was realized using highly active but toxic aqueous bromine oxidant[10]. The present power performance can also compete with state-of-the-art practices of PEM fuel cells[34], thus, the new cell shows great promise in powering a variety of applications.

3.3 Recharging and round-trip efficiency

Charging behaviors were investigated in Figure 3(a). As shown in the figure, water electrolysis in the s-URFC shifts its onset voltage down to 0.57 V, which is less than half those of the single-pH cells. At 1.2 V, the s-URFC was found to split water at a current density of 0.8 A cm^{-2}, yet, to achieve the same performance, voltage inputs > 2 V are required for both the single-pH cases. The corresponding individual anode and cathode performances in Figure 3(b) show that the thermodynamic advantage is the major contributor to the performance enhancement whereas the electrode kinetics in alkaline and acid electrolytes exhibit only slight difference. With the voltage contributions from the electrochemical neutralization reaction as a result of the switchable pH-differential arrangement, the s-URFC exhibits voltage efficiencies >100%. Voltage efficiencies of 253% and 114% were observed respectively at current densities of 0.1 A cm^{-2} and 0.6 A cm^{-2} (corresponding to 12% and 59% of peak power, respectively). To evaluate the round-trip efficiency of power-to-fuel-to-power in the present system, the consumption of base and acid by the electrochemical neutralization are taken into account as follows (refer to Supplementary for derivation details)

$$\eta = U_{FC}/(U_{EL} + 2U_{EN}) \quad (1)$$

where U denotes voltage, the subscripts FC, EL and EN respectively denote fuel cell, electrolysis and electrochemical neutralization. Here the acid-base neutralization at the electrolyte-electrolyte interface is not included in view of its associated negligible reactant loss as demonstrated by fluorescence microscopy. Figure 3(c) compares the round-trip efficiency of the s-URFC with those of the single-pH cells. It is seen that the efficiency curve of the s-URFC is well above those of the single-pH cells over the range of measured currents. In all the three cells, the efficiency gradually decreases with increasing current density because overpotentials are directly proportional to the operating current density. At 0.04 A cm^{-2} (3.1% of peak power), the s-URFC gives an efficiency of 74%, which appears to be the highest round-trip efficiency for H_2/O_2 URFC to date, though most of the previous data were obtained at elevated temperatures (> 80 ^oC) and pressures (2~3 atm) (Figure 3(d))[35-49].

3.4 Cycling performance

In addition to the electrochemical performances, cycling durability is another important performance indicator for a RFC. The cycling performance of the s-URFC was studied using galvanostatic measurements at a current density of 0.1 A cm^{-2} (Figure 4(a)). No significant performance degradation was observed after a 10-hr cycle period. SEM micrographs in the insets also show no obvious change in surface morphology of the electrode carbon support before or after cycling. Separate CV tests of the PtRu/C catalysts were further conducted under acid and alternating acid-base conditions to investigate the effect of the alternating pH environments on its catalytic activity. As shown in Figures 4(b2) and 4(b4), the absorption peaks of hydrogen in the two cases undergo a similar decrease (14% for acid, and 19% for alternating acid-base) after 105 CV cycles as a result of a decrease of catalytic surface area. The activity loss is attributable to the dissolution of PtRu nanoparticles[50], which is in reasonable agreement with particle size distributions estimated from TEM data in Figure 4(b6).

The particle sizes change slightly from their original distribution after cycling, whereas no significant change is found in the distributions with different cycling conditions. The above results suggest that the proposed electrolyte switching strategy does not introduce additional difficulties for catalyst development, meaning that catalysts for the conventional unitized-type RFCs are also applicable to our s-URFC.

4 Discussion

It is worth studying the energy loss mechanisms in the new cell so as to find strategies to further improve the cell design. Energy in electrochemical systems is generally lost in three forms of heat, including irreversible heat of the electrochemical reaction, reversible entropic heat and ohmic Joule heat. In the s-URFC, heat will also be generated due to the interfacial acid-base neutralization which is an exothermic reaction. Temperature is the most suitable indicator to reflect the amount of heat dissipated. Therefore, to identify and compare the heat loss mechanisms between an s-URFC and a single electrolyte cell, temperature is selected as an indicator, which can be determined and recorded by infrared microscopy. Noted that 'temperature' is not an influencing factor that could affect the cell performance, but an indicator to help visualize and map the heat loss in the system. Figure 5(a) compares the thermographs of the s-URFC and its single-acid counterpart operated in the EL mode. As expected, in the single-acid case, the region adjacent to the anode (i.e., oxygen electrode) is subject to the highest local temperatures, indicating the severest loss associated with the oxygen evolution reaction. For the s-URFC, a temperature rise occurs in both electrode and acid-base interfacial regions. At low current densities (< 0.02 A cm^{-2}), the interfacial heat is dominant, while the electrode heat becomes notable as the current density increases. Interestingly, the electrode loss (particularly the anode loss) in the s-URFC is much less compared to that in the single acid cell. This can be explained by the fact that the operation of the s-URFC is much closer to the

equilibrium status (corresponding to less electrode overpotentials) than the single-acid cell at the same current densities, requiring lower electron transfer overpotential, which is the potential difference above the equilibrium value. Therefore, a good control of the interfacial heat generation is the key to any future improvement of the s-URFC. According to Figure 5(b1), increasing the electrolyte flow rate can effectively suppress the temperature increase at the acid-base interface. This is due partly to an enhanced heat removal at larger flow rates, and partly to a thinner interfacial mixing layer as a result of increased flow rates. The acid-base neutralization is known to be a superfast reaction with a rate constant ~10^{11} M^{-1} s^{-1}, which is 2~3 orders of magnitude higher than the diffusion rate of proton / hydroxyl ions. Thus, the interfacial neutralization is determined by the mixing process, and the thickness of the neutralization reaction zone should be equal to that of the mixing layer. Figure 5(b2) confirms that the interfacial layer thickness decreases from 1000 μm to 200 μm as the electrolyte flow rate increases from 400 μL min^{-1} to 2000 μL min^{-1}. In this regard, our previous membraneless cell designs that are able to minimize the interfacial mixing, such as the counter-flow design[51, 52] and thermodynamic focusing design[53], are likely to benefit the performance of the s-URFC. In a normal bipolar membrane configuration[14, 15], the neutralization of the alkaline and acidic electrolytes will also occur, and a regeneration step is still needed. Same as our membraneless configuration, the neutralization in a normal bipolar membrane-based cell is contributed by both bulk neutralization and electrochemical neutralization processes. It is difficult to control the electrochemical neutralization in any pH-differential electrochemical systems as it is related to the overall cell reactions. However, in contrast to the normal membrane-based configuration, the bulk neutralization can be well minimized with the present configuration by tuning the hydrodynamic conditions. By using fluorescence microscopy and infrared imaging, we demonstrated that the acid-base interface thickness is well controlled in an s-URFC and the interfacial neutralization reaction, though happens, is suppressed in its

extent. Thus, the consumed portion of H^+ and OH^-, and the heat loss due to the neutralization reaction could be minimized to a low level. It should also be noted that the exit anolyte and catholyte can be collected separately. With low degradation mentioned above, electrolyte reuse is achievable by minor ion replenishment. Following the scaling-out method discussed in our previous work[54], the s-URFC is readily scalable to meet energy requirements of applications at different scales. Besides, operation parameters of a microfluidic network, such as catalyst to Nafion ratio, dimensions of catalyst exposure area, microchannel thickness, electrolyte flow rate and concentration, and H_2/O_2 supply rate and pressure, would affect the reactor performance to a certain extent. Therefore, continued experimental analysis is worthwhile for a comprehensive understanding of the intrinsic correlations, thus further optimizing the performance. Apart from the cell design improvement, the demonstrated performance-enhancing principle also opens up opportunities for new energy technologies. For instance, industrial waste acids and alkalis can be used as low-cost feed stocks by our system for high-quality electricity production. Moreover, with the present platform, other similar strategies (e.g., concentration differential) might also be used to achieve high electrochemical performance and efficiency through adjusting thermodynamic electrochemical window.

5 Conclusions

In this study, we for the first time propose to overcome the limitations of the existing regenerative hydrogen / oxygen fuel cell technologies by using a switchable pH-differential strategy. Although the design and operating parameters have not been optimized, the present cell outperforms the best PEM water electrolyzer to date when operated in the EL mode, and rivals the state-of-the-art performance of PEM fuel cells when operated in the FC mode, but with a much cheaper and lighter unitized configuration. The cell allows an access to very low charging voltages and very high discharge voltages, and it has a round-trip efficiency up to

74%. The new system also shows good compatibility with the existing bifunctional electrocatalysts by running stably on commercial PtRu catalysts over a 10-hr cycle period. The proposed switchable pH-differential strategy in the study is complementary to other ongoing efforts (such as material development) in developing high-performance energy storage technologies, and we believe that the new cell together with advances in catalyst materials will play an important role in addressing the rapidly growing need for high-capacity, efficient and low-cost energy storage.

Acknowledgements

This research was supported by the Hong Kong Research Grant Council GRF#714313, Scottish Funding Council / Research Grants Council Joint Research Scheme H15009, and National Natural Science Foundation of China #51406057.

References

[1] P. Millet, R. Ngameni, S. Grigoriev, V. Fateev, international journal of hydrogen energy, 36 (2011) 4156-4163.

[2] M.Y. Suberu, M.W. Mustafa, N. Bashir, Renewable and Sustainable Energy Reviews, 35 (2014) 499-514.

[3] M.K. Debe, Nature, 486 (2012) 43-51.

[4] I.H. Hafez, M.R. Berber, T. Fujigaya, N. Nakashima, Scientific reports, 4 (2014).

[5] M.A. Hoque, F.M. Hassan, D. Higgins, J.Y. Choi, M. Pritzker, S. Knights, S. Ye, Z. Chen, Advanced Materials, 27 (2015) 1229-1234.

[6] H. Wang, Y. Liang, Y. Li, H. Dai, Angewandte Chemie International Edition, 50 (2011) 10969-10972.

[7] Y. Liang, Y. Li, H. Wang, J. Zhou, J. Wang, T. Regier, H. Dai, Nature materials, 10 (2011) 780-786.

[8] H. Wang, Y. Yang, Y. Liang, G. Zheng, Y. Li, Y. Cui, H. Dai, Energy & Environmental Science, 5 (2012) 7931-7935.

[9] Y. Li, W. Zhou, H. Wang, L. Xie, Y. Liang, F. Wei, J.-C. Idrobo, S.J. Pennycook, H. Dai, Nature nanotechnology, 7 (2012) 394-400.

[10] W.A. Braff, M.Z. Bazant, C.R. Buie, Nature communications, 4 (2013).

[11] Y. Chen, A. Lavacchi, H. Miller, M. Bevilacqua, J. Filippi, M. Innocenti, A. Marchionni, W. Oberhauser, L. Wang, F. Vizza, Nature communications, 5 (2014).

[12] F.R. Brushett, M.S. Naughton, J.W.D. Ng, L. Yin, P.J. Kenis, international journal of hydrogen energy, 37 (2012) 2559-2570.

[13] S.A.M. Shaegh, N.-T. Nguyen, S.H. Chan, International Journal of Hydrogen Energy, 36 (2011) 5675-5694.

[14] M. Ünlü, J. Zhou, P.A. Kohl, The Journal of Physical Chemistry C, 113 (2009) 11416-11423.

[15] H. Li, G. Weng, C.Y.V. Li, K.-Y. Chan, Electrochimica Acta, 56 (2011) 9420-9425.

[16] P. Chaurasia, Y. Ando, T. Tanaka, Energy conversion and Management, 44 (2003) 611-628.

[17] H. Takenaka, E. Torikai, Y. Kawami, N. Wakabayashi, International Journal of Hydrogen Energy, 7 (1982) 397-403.

[18] E.R. Choban, J. Spendelow, L. Gancs, A. Wieckowski, P. Kenis, Electrochimica Acta, 50 (2005) 5390-5398.

[19] J. Zhang, Y. Tang, C. Song, J. Zhang, H. Wang, Journal of power sources, 163 (2006) 532-537.

[20] M.S. Naughton, A.A. Moradia, P.J. Kenis, Journal of the Electrochemical Society, 159 (2012) B761-B769.

[21] R. Ferrigno, A.D. Stroock, T.D. Clark, M. Mayer, G.M. Whitesides, Journal of the American Chemical Society, 124 (2002) 12930-12931.

[22] E.R. Choban, L.J. Markoski, A. Wieckowski, P.J. Kenis, Journal of Power Sources, 128 (2004) 54-60.

[23] S. Hasegawa, K. Shimotani, K. Kishi, H. Watanabe, Electrochemical and Solid-State Letters, 8 (2005) A119-A121.

[24] R.S. Jayashree, D. Egas, J.S. Spendelow, D. Natarajan, L.J. Markoski, P.J. Kenis, Electrochemical and Solid-State Letters, 9 (2006) A252-A256.

[25] R.S. Jayashree, L. Gancs, E.R. Choban, A. Primak, D. Natarajan, L.J. Markoski, P.J. Kenis, Journal of the American Chemical Society, 127 (2005) 16758-16759.

[26] E. Kjeang, B.T. Proctor, A.G. Brolo, D.A. Harrington, N. Djilali, D. Sinton, Electrochimica Acta, 52 (2007) 4942-4946.

[27] R.S. Jayashree, M. Mitchell, D. Natarajan, L.J. Markoski, P.J. Kenis, Langmuir, 23 (2007) 6871-6874.

[28] E. Kjeang, R. Michel, D.A. Harrington, N. Djilali, D. Sinton, Journal of the American Chemical Society, 130 (2008) 4000-4006.

[29] E. Kjeang, A.G. Brolo, D.A. Harrington, N. Djilali, D. Sinton, Journal of the Electrochemical Society, 154 (2007) B1220-B1226.

[30] E. Kjeang, R. Michel, D.A. Harrington, D. Sinton, N. Djilali, Electrochimica Acta, 54 (2008) 698-705.

[31] S. Cheng, K.-Y. Chan, ECS Transactions, 25 (2010) 213-219.

[32] N.D. Mota, D.A. Finkelstein, J.D. Kirtland, C.A. Rodriguez, A.D. Stroock, H.c.D. Abruña, Journal of the American Chemical Society, 134 (2012) 6076-6079.

[33] S.A.M. Shaegh, N.-T. Nguyen, S.H. Chan, Journal of Power Sources, 209 (2012) 312-317.

[34] H. Zhang, P.K. Shen, Chemical Society Reviews, 41 (2012) 2382-2394.

[35] M.J. Lavorante, L.G. Messina, J.I. Franco, P. Bonelli, International Journal of Hydrogen Energy, 39 (2014) 8631-8634.

[36] F. Mitlitsky, B. Myers, A.H. Weisberg, Energy & Fuels, 12 (1998) 56-71.

[37] S. Zhigang, Y. Baolian, H. Ming, Journal of power sources, 79 (1999) 82-85.

[38] T. Ioroi, N. Kitazawa, K. Yasuda, Y. Yamamoto, H. Takenaka, Journal of Applied Electrochemistry, 31 (2001) 1179-1183.

[39] T. Ioroi, K. Yasuda, Z. Siroma, N. Fujiwara, Y. Miyazaki, Journal of Power sources, 112 (2002) 583-587.

[40] S.-D. Yim, W.-Y. Lee, Y.-G. Yoon, Y.-J. Sohn, G.-G. Park, T.-H. Yang, C.-S. Kim, Electrochimica Acta, 50 (2004) 713-718.

[41] D.J. Bents, V.J. Scullin, B.-J. Chang, D.W. Johnson, C.P. Garcia, in: 2004 Fuel Cell Seminar, San Antonio, TX, November, 2004, pp. 1-5.

[42] S.-D. Yim, G.-G. Park, Y.-J. Sohn, W.-Y. Lee, Y.-G. Yoon, T.-H. Yang, S. Um, S.-P. Yu, C.-S. Kim, International Journal of Hydrogen Energy, 30 (2005) 1345-1350.

[43] Y. Zhang, C. Wang, N. Wan, Z. Mao, International Journal of Hydrogen Energy, 32 (2007) 400-404.

[44] H.-Y. Jung, S. Park, B.N. Popov, Journal of Power Sources, 191 (2009) 357-361.

[45] G. Chen, H. Zhang, H. Zhong, H. Ma, Electrochimica Acta, 55 (2010) 8801-8807.

[46] Y. Zhang, H. Zhang, Y. Ma, J. Cheng, H. Zhong, S. Song, H. Ma, Journal of Power Sources, 195 (2010) 142-145.

[47] S. Altmann, T. Kaz, K.A. Friedrich, Electrochimica Acta, 56 (2011) 4287-4293.

[48] A. Ranjbari, P. Millet, S. Grigoriev, V. Fateev, D. Stolten, T. Grube, Report Nr.: Schriften des Forschungszentrums Jülich/Energy & Environment, (2010).

[49] S.-Y. Huang, P. Ganesan, H.-Y. Jung, B.N. Popov, Journal of Power Sources, 198 (2012) 23-29.

[50] L. Jörissen, Journal of Power Sources, 155 (2006) 23-32.

[51] J. Xuan, D.Y. Leung, M.K. Leung, H. Wang, M. Ni, Journal of Power Sources, 196 (2011) 9391-9397.

[52] H. Xu, H. Zhang, H. Wang, D.Y. Leung, L. Zhang, J. Cao, K. Jiao, J. Xuan, Applied Energy, (2015).

[53] B. Zhang, D.-d. Ye, P.-C. Sui, N. Djilali, X. Zhu, Journal of Power Sources, 259 (2014) 15-24.

[54] H. Wang, S. Gu, D.Y. Leung, H. Xu, M.K. Leung, L. Zhang, J. Xuan, Electrochimica Acta, 135 (2014) 467-477.

Table 1. Reactions in the s-URFC

	Fuel cell mode	Electrolysis mode
Cathode[a]	$O_2 + 4H^+ + 4e^- \rightarrow 2H_2O$	$4OH^- \rightarrow 2H_2O + O_2 + 4e^-$
	$E^0 = 1.257$ V vs. SHE	$E^0 = 0.375$ V vs. SHE
Anode[b]	$2H_2 + 4OH^- \rightarrow 4H_2O + 4e^-$	$2H^+ + 2e^- \rightarrow H_2$
	$E^0 = -0.854$ V vs SHE	$E^0 = 0.028$ V vs SHE
Overall	$2H_2 + O_2 + 4OH^- + 4H^+ \rightarrow$	$4OH^- + 2H^+ \rightarrow 2H_2O + H_2 + O_2$
	$2H_2O + 4H_2O$ $E^0 = 2.111$ V	$E^0 = 0.347$ V

[a] In 3 M H_2SO_4. [b] In 3 M KOH.

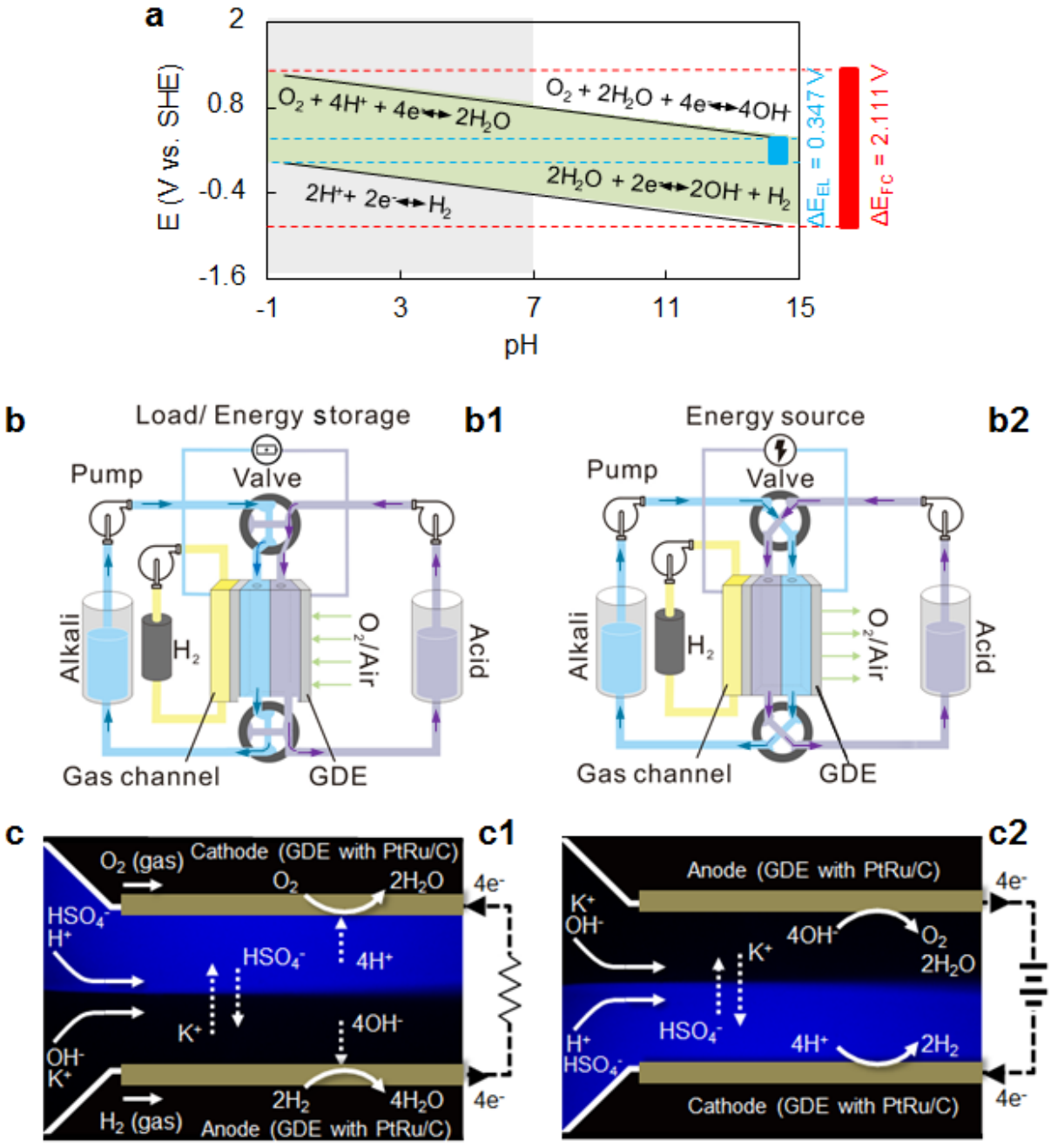

Figure 1 Working principles of the s-URFC. (**a**) Pourbaix diagram of water at 25°C and 1 atm to illustrate the idea behind the work. (**b**) Schematic representation of the proposed s-URFC system operating in the (**b1**) FC and (**b2**) EL modes. (**c**) Reactant flow within the s-URFC in the (**c1**) FC and (**c2**) EL modes. The contours reflect the pH distributions inside the

cell captured by a fluorescent microscope when flowing 3 M H_2SO_4 and 3 M KOH side by side at a stream flow rate of 1400 μL min^{-1}.

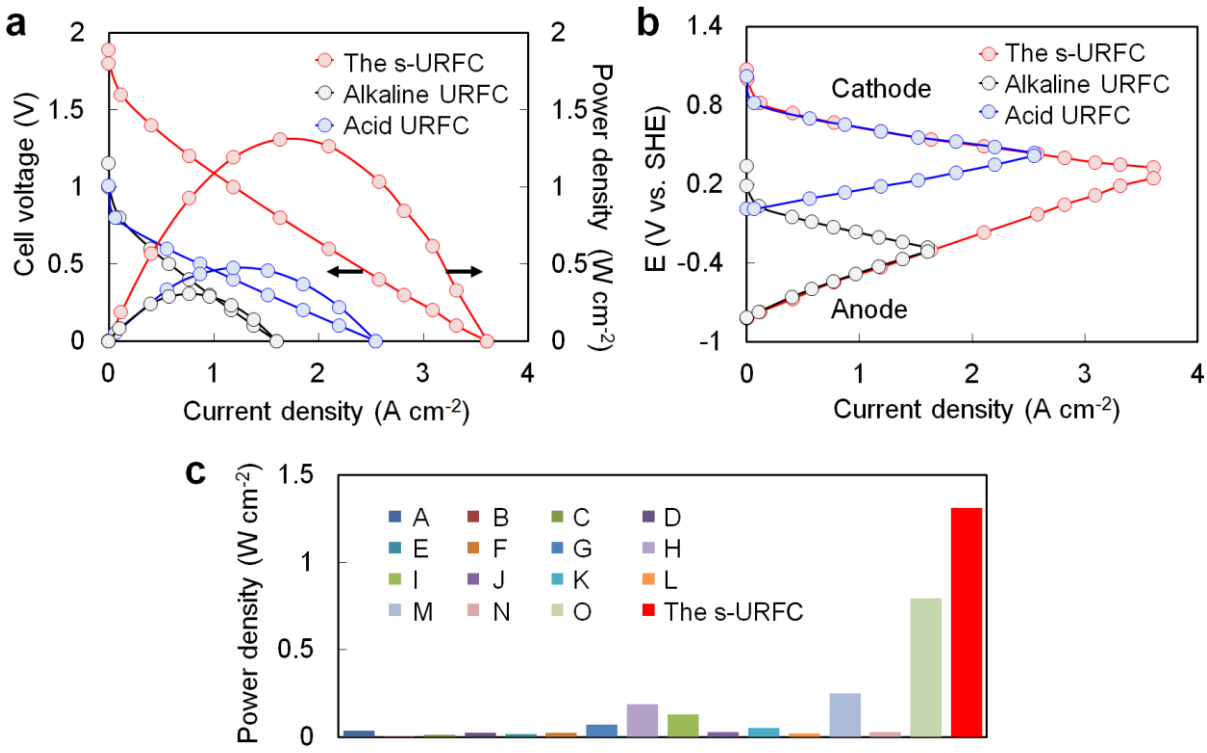

Figure 2. Discharge performance of the s-URFC. (a) Polarization curves and (b) the corresponding individual electrode polarization curves of the s-URFC compared with single-electrolyte counterparts. (c) Performance comparison of the s-URFC and other membraneless laminar-based flow fuel cells in literatures (A-O). A: Harvard University, 2002[21]; B: University of Illinois at Urbana-Champaign, 2004[22]; C: University of Illinois at Urbana-Champaign, 2005[18]; D: Fuji Xerox Company, 2005[23]; E: University of Illinois at Urbana-Champaign, 2006[24]; F: University of Illinois at Urbana-Champaign, 2005[25]; G: University of Victoria, 2007[26]; H: University of Illinois at Urbana-Champaign, 2007[27]; I: University of Victoria, 2008[28]; J: University of Victoria, 2007[29]; K: University of Victoria, 2008[30]; L: University of Hong Kong, 2010[31]; M: Cornell University, 2012[32]; N: Nanyang Technological University, 2012[33]; O: Massachusetts Institute of Technology, 2013[10].

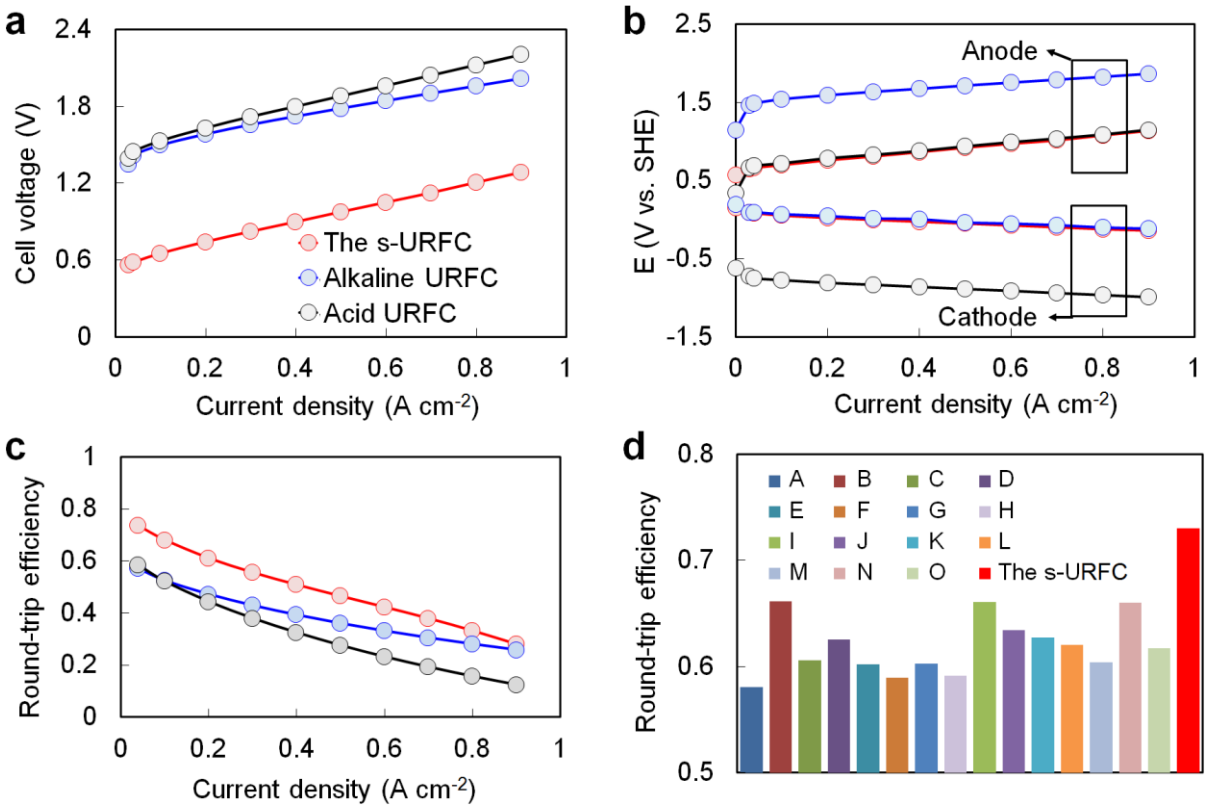

Figure 3. Charging performance of the s-URFC. (a) Polarization curves and (b) the corresponding individual electrode polarization curves of the s-URFC compared with single-electrolyte counterparts. (c) Round-trip voltage efficiency. (d) Comparison of the present s-URFC and other hydrogen/oxygen regenerative cells in terms of round-trip voltage efficiency (A-O). A: The National Aeronautics and Space Administration, 1996[35]; B: The National Aeronautics and Space Administration, 1997[36]; C: Chinese Academy of Sciences, 1999[37]; D: The National Institute of Advanced Industrial Science and Technology, 2001[38]; E: The National Institute of Advanced Industrial Science and Technology, 2002[39]; F: Korea Institute of Energy Research, 2004[40]; G: NASA, 2005[41]; H: Korea Institute of Energy Research, 2005[42]; I: Tsinghua University, 2007[43]; J: University of South Carolina, 2009[44]; K: Chinese Academy of Sciences, 2010[45]; L: Chinese Academy of Sciences, 2010[46]; M:

University Stuttgart & German Aerospace Centre, 2011[47]; N: University of Paris & Kurchatov Institute, 2010[48]; O: University of South Carolina, 2012[49].

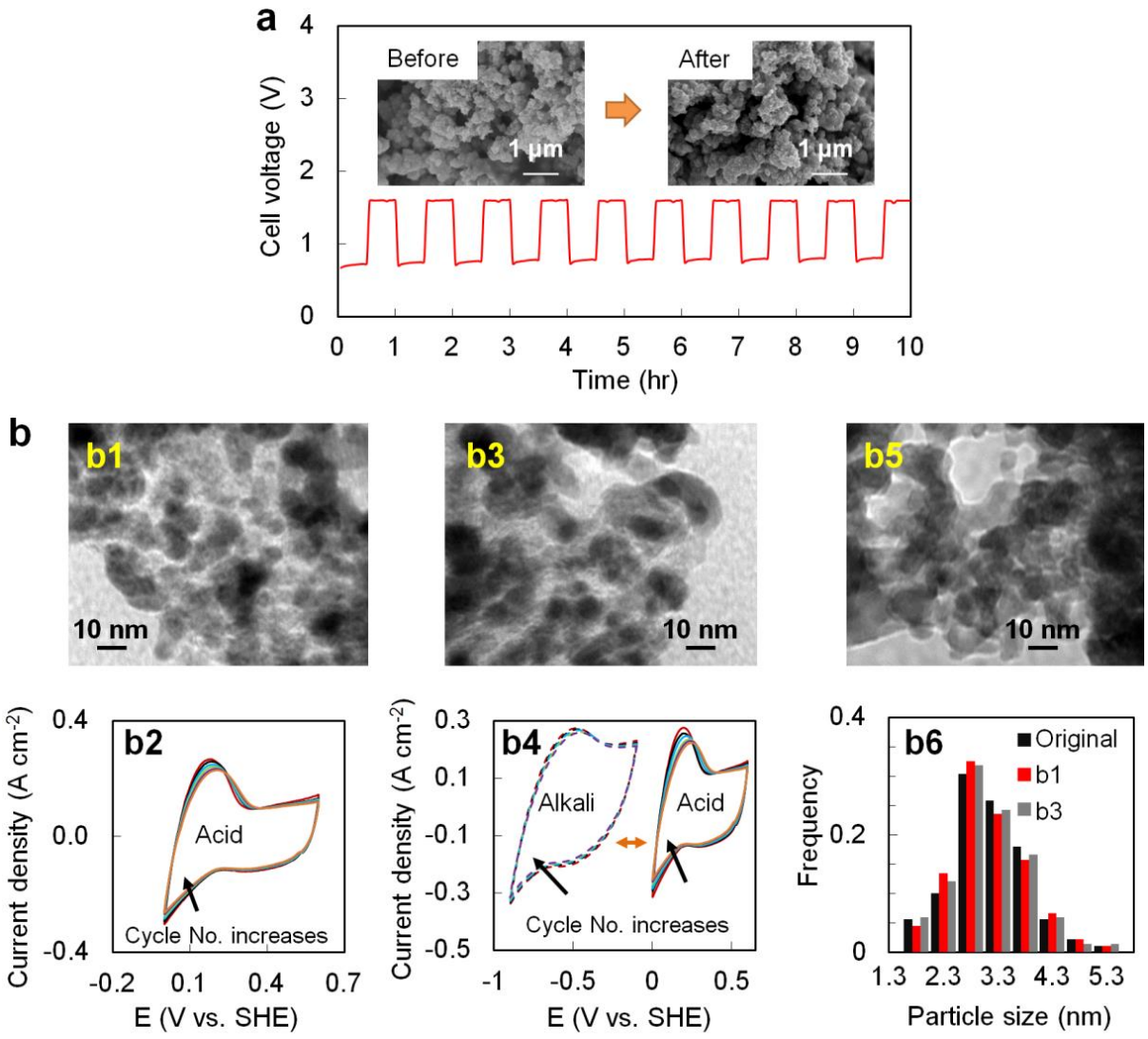

Figure 4 Cycling performances of the s-URFC. (**a**) Galvanostatic charge and discharge curves of the s-URFC at a current density of 0.1 A cm^{-2} in a 10-h cycle period. Each cycle lasts for 1 hour, containing half-hour operation in the FC mode and half-hour operation in the EL mode. Insets show the SEM characterization of the electrode carbon substrate before and after cycling. (**b**) Cycling stability of PtRu/C catalysts under different pH conditions: **(b1**) TEM image of the catalysts after 105 CV cycles in 3 M H_2SO_4 and (**b2**) its associated CV curves at the 5^{st}, 25^{th}, 45^{th}, 65^{th}, 85^{th} and 105^{th} cycle; **(b3**) TEM image of the catalysts after 105 CV

cycles in alternating 3 M H_2SO_4 / 3 M KOH environments and (**b4**) its associated CV curves at the 5st, 25th, 45th, 65th, 85th and 105th cycle; (**b5**) TEM image of the catalysts before CV cycling; (**b6**) Particle size distributions before and after the CV cycling under different conditions.

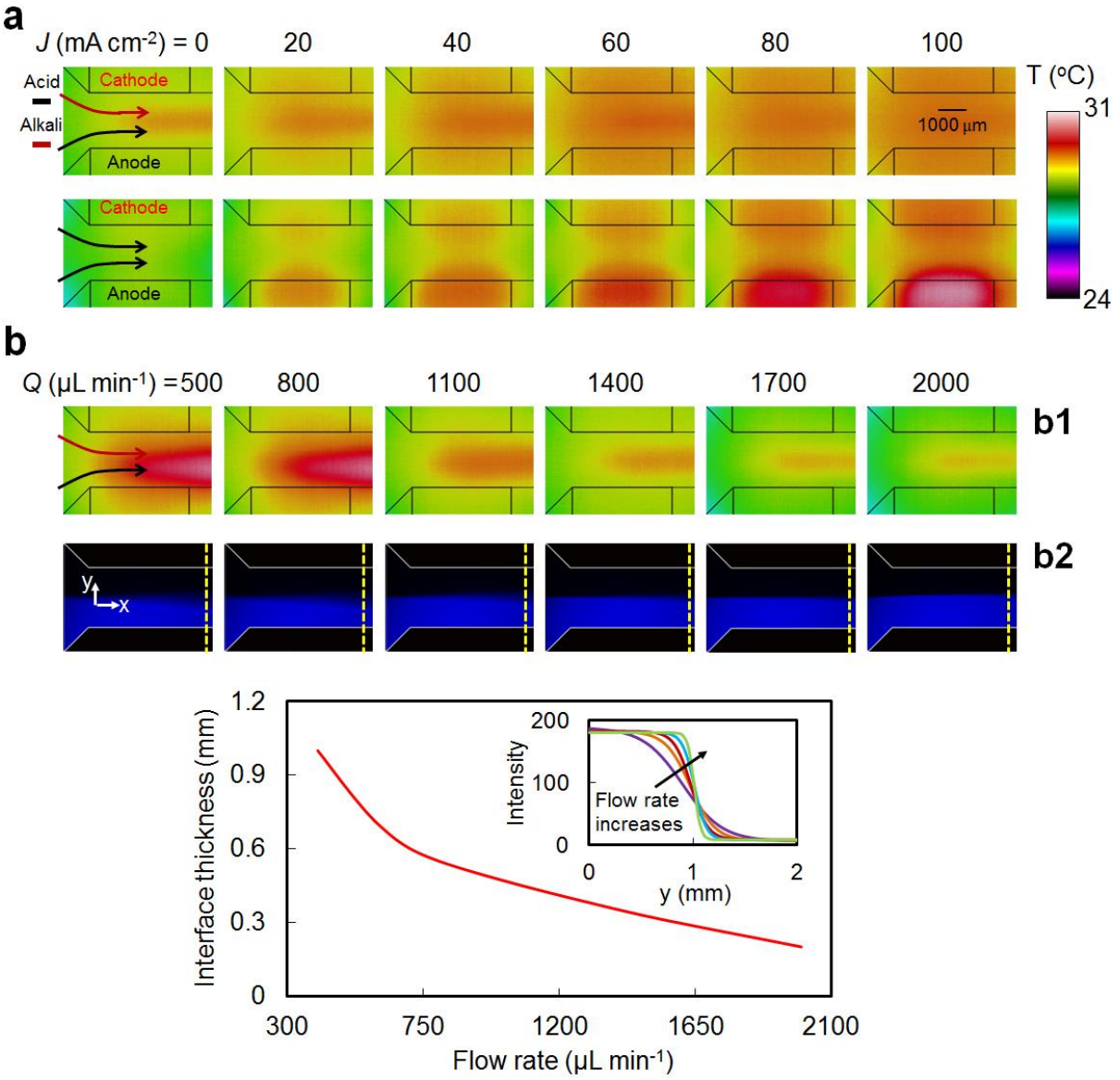

Figure 5 Loss mechanisms in the s-URFC. (**a**) Temperature distributions within the microchannel of an s-URFC and a single acid cell at different current densities and the electrolyte flow rate of 1400 μL min^{-1}. (**b**) (**b1**) Temperature distributions within the microchannel of an s-URFC at different electrolyte flow rates under an open-circuit condition;

(**b2**) Thickness of the acid-base interface as a function of flow rate under an open-circuit condition. All the measurements were performed by operating the cell in the EL mode.